Ultrasonics 54 (2014) 137–146

Contents lists available at SciVerse ScienceDirect

Ultrasonics

journal homepage: www.elsevier.com/locate/ultras

Lesion edge preserved direct average strain estimation for ultrasound elasticity imaging

Mohammad Arafat Hussain [a], Farzana Alam [b], Sharmin Akhtar Rupa [c], Rayhana Awwal [d], Soo Yeol Lee [e], Md. Kamrul Hasan [a,e,*]

[a] Department of Electrical and Electronic Engineering, Bangladesh University of Engineering and Technology, Dhaka 1000, Bangladesh
[b] Department of Radiology and Imaging, Bangabandhu Sheikh Mujib Medical University, Dhaka 1000, Bangladesh
[c] Department of Radiology and Imaging, Enam Medical College and Hospital, Savar, Dhaka, Bangladesh
[d] Department of Plastic Surgery and Burn Unit, Dhaka Medical College and Hospital, Dhaka 1000, Bangladesh
[e] Department of Biomedical Engineering, Kyung Hee University, 1 Seochun, Yongin-si, Gyeonggi-do 446-701, Republic of Korea

ARTICLE INFO

Article history:
Received 16 September 2012
Received in revised form 9 May 2013
Accepted 20 May 2013
Available online 10 June 2013

Keywords:
Elastography
Ultrasonic imaging
Instantaneous strain
Average strain
Normalized cross-correlation

ABSTRACT

Elasticity imaging techniques with built-in or regularization-based smoothing feature for ensuring strain continuity are not intelligent enough to prevent distortion or lesion edge blurring while smoothing. This paper proposes a novel approach with built-in lesion edge preservation technique for high quality direct average strain imaging. An edge detection scheme, typically used in diffusion filtering is modified here for lesion edge detection. Based on the extracted edge information, lesion edges are preserved by modifying the strain determining cost function in the direct-average-strain-estimation (DASE) method. The proposed algorithm demonstrates approximately 3.42–4.25 dB improvement in terms of edge-mean-square-error (EMSE) than the other reported regularized or average strain estimation techniques in finite-element-modeling (FEM) simulation with almost no sacrifice in elastographic-signal-to-noise-ratio (SNRe) and elastographic-contrast-to-noise-ratio (CNRe) metrics. The efficacy of the proposed algorithm is also tested for the experimental phantom data and *in vivo* breast data. The results reveal that the proposed method can generate a high quality strain image delineating the lesion edge more clearly than the other reported strain estimation techniques that have been designed to ensure strain continuity. The computational cost, however, is little higher for the proposed method than the simpler DASE and considerably higher than that of the 2D analytic minimization (AM2D) method.

1. Introduction

Elastography is an emerging medical imaging modality for detecting the abnormal changes in soft tissue via the assessment of tissue stiffness usually in terms of strain. It can be considered an alternative to manual palpation of tissue, practiced by physicians for primary clinical diagnosis. Generally, pathologic and stiffness changes in soft tissue are well-correlated, and therefore, abnormal changes in stiffness convey warning signs of diseases in organs like breast, liver, and prostate [9,17,18]. In quasi-static elastography, various strain estimation methods have been developed for the detection and classification of lesions and/or tissue pathology change. Some of them are gradient-based techniques [1,8,15,17,18,25] where the strain is typically computed as the spatial gradient of local tissue displacements, and some are direct-strain-estimation techniques [3,16,23] where the strain is directly estimated from the pre- and post-compression RF echo waveforms or spectra.

The gradient-based strain estimators face challenges in maintaining displacement continuity due to pre- and post-compression echo decorrelation, and other noise artifacts [3,8,16]. The gradient operation over the displacement map further amplifies these high frequency noise while estimating strain [1,23]. To obtain a noise reduced strain map, a smoothing technique based on least-squares-linear-regression [13] or least-squared-error-based smoothing-spline [1] can be applied on the displacement matrix before the gradient operation. In addition, some of the recent methods designed to ensure displacement continuity (and thus strain continuity) use estimates from the previous window in estimating the interrogated window displacement [20–22,25]. In all these techniques, strain continuity is achieved only at the cost of lesion edge blurring along with the smoothing of the natural stiffness variation inside the lesion.

Noise in the strain map resulting from the derivative operation in the gradient-based methods can be avoided by using direct-strain-estimation methods that exist both in the time [3,11] and frequency domain [10,23]. Though these methods show better

* Corresponding author at: Department of Electrical and Electronic Engineering, Bangladesh University of Engineering and Technology, Dhaka 1000, Bangladesh. Tel.: +880 2 966 5650.
E-mail address: khasan@eee.buet.ac.bd (M.K. Hasan).

0041-624X/$ - see front matter © 2013 Elsevier B.V. All rights reserved.
http://dx.doi.org/10.1016/j.ultras.2013.05.010

SNRe performance than the gradient-based techniques, they also face challenges to ensure strain continuity among neighborhood due to echo decorrelation. To ensure strain continuity, in [10,11], a cost function is defined for an interrogated point on the strain map from its exponentially weighted neighboring window pre- and post-compression RF spectral sum-of-square-differences (SSD) or echo cross-correlation peaks, respectively, in both the axial and lateral directions. However, though lesion edge preservation while ensuring the strain continuity is of great importance, none of these techniques are intelligent enough to detect and preserve the lesion edge as well as its natural stiffness variation inside.

In this paper, we propose a lesion edge preserved direct average strain estimation (LEP-DASE) method for elastography. We modify the direct average strain estimation (DASE) technique proposed in [11] by introducing a built-in edge preservation criterion into the average strain estimating cost function. A modified scheme based on [14] is proposed here for lesion edge detection. The performance of this algorithm is evaluated using a FEM phantom, experimental phantom as well as *in vivo* patient data, and compared with other recently reported regularized strain estimation algorithms.

The paper is organized as follows. Section 2 describes the basic DASE and proposed LEP-DASE techniques. Section 3 presents the simulation and experimental results to demonstrate the strength of the proposed algorithm. Section 4 presents a discussion on the study and concluding remarks are given in Section 5.

2. Methods

2.1. Brief Review of the Direct Average Strain Estimation

The simplified 1-D model of the backscattered ultrasound RF signals before and after compression are given by [3]:

$$r_1(t) = s_1(t) + v_1(t) = s(t) * p(t) + v_1(t), \tag{1}$$

$$r_2(t) = s_2(t) + v_2(t) = s\left(\frac{t}{a} - t_0\right) * p(t) + v_2(t), \tag{2}$$

where $s(t)$ denotes the 1-D scattering function of the elastic target, $p(t)$ denotes the point-spread-function (PSF), a denotes the compression factor due to axial deformation of the target medium, t_0 denotes the time delay, $v_1(t)$ and $v_2(t)$ denote the uncorrelated random noise profiles, $r_1(t)$ and $r_2(t)$ denote the pre- and post-compression rf echo signals, respectively, and $*$ indicates the convolution operation. The strain s is related to the compression factor $1/a$ as [4], $s = 1 - a$ where $a \leqslant 1$ and $s \ll 1$.

Hussain et al. [11] proposed a method for direct average strain estimation (DASE) using the weighted nearest neighbor method in order to compensate for the signal de-correlation due to non-axial motion of tissue scatterers and thereby to introduce a built-in smoothing feature in the strain estimation algorithm. Calculated strain from a pair of windowed RF segments for a particular tissue point is assumed to be similar to the strains in the neighboring tissues due to their physical proximity. This assumption, however, works well unless there is a sudden change in the tissue stiffness.

Let $F_1(i,j)$ and $F_2(i,j)$ are the pre- and post-compression ultrasound RF echo frames, respectively. Here, i is the axial depth index and j is the RF A-line index. An effective strain at a point $(i_s j_s)$ on the strain map can be estimated from a corresponding pair of 1-D windowed RF segments $r_1^{(i_s j_s)}$ and $r_2^{(i_s j_s)}$ selected from the pre- and post-compression ultrasound image frames as [11]

$$r_1^{(i_s j_s)}(i) = F_1((i_s - 1)L_v + i, j), \quad \text{for} \quad 1 \leqslant i \leqslant L_i \text{ and } j = j_s \tag{3}$$

$$r_2^{(i_s j_s)}(i) = F_2(round((i_s - 1)(1 - s_{avg})L_v) + i, j), \quad \text{for} \quad 1 \leqslant i \leqslant L_i$$
$$\text{and } j = j_s + \left(j_s - \frac{N_c}{2}\right)s_{avg}v \tag{4}$$

where v represents the Poisson's ratio, N_c represents the number of scan lines in the RF frame, L_v is the axial separation between two successive RF windows in samples and L_i represents the length of the 1-D RF window. The assumption that the approximate applied strain s_{avg} is known a priori is a drawback of the DASE method [11]. In this paper, instead of assuming that s_{avg} is a known constant, we adaptively define it from the estimated previous window strain $S_o(i_s - 1, j_s)$ as [6]

$$s_{avg} = \begin{cases} 0; & i_s = 1 \\ S_o(i_s - 1, j_s); & \text{otherwise.} \end{cases} \tag{5}$$

After stretching the post-compression echo segment $r_2^{(i_s j_s)}$ by a factor α ($\leqslant 1$), the normalized cross-correlation (NCC) coefficient $\rho_\alpha(k)$ between $r_1^{(i_s j_s)}$ and $r_\alpha^{(i_s j_s)}$ is estimated as [19],

$$\rho_\alpha^{(i_s j_s)}(k) = \frac{\sum_{i=1}^{L_i} r_1^{(i_s j_s)}(i) \cdot r_\alpha^{(i_s j_s)}(i+k)}{\sqrt{\sum_{i=1}^{L_i}\{r_1^{(i_s j_s)}(i)\}^2 \sum_{i=1}^{L_i}\{r_\alpha^{(i_s j_s)}(i)\}^2}}. \tag{6}$$

The peaks of $\rho_\alpha^{(i_s j_s)}(k)$ are calculated by using the cosine interpolation for different values of α:

$$M_\alpha(i_s, j_s) = \rho_\alpha^{(i_s j_s)}\left(\arg\max_k\{\rho_\alpha^{(i_s j_s)}(k)\}\right), \tag{7}$$

where M_α is a matrix that contains the NCC peaks. For average strain estimation, a cost function is defined as

$$J_\alpha^{(i_s j_s)} = \sum_{i_0 = i_s - L_a}^{i_s + L_a} \sum_{j_0 = j_s - L_l}^{j_s + L_l} w^{(i_s j_s)}(i_0, j_0) M_\alpha(i_0, j_0), \tag{8}$$

where

$$w^{(i_s j_s)}(i_0, j_0) = e^{-|\lambda_a(i_0 - i_s)| - |\lambda_l(j_0 - j_s)|}, \text{ for } i_s - L_a \leqslant i_0 \leqslant i_s + L_a; j_s - L_l \leqslant j_0 \leqslant j_s + L_l \tag{9}$$

Here, λ_a and λ_l are the weighting factors, and L_a and L_l are the nearest neighbor (NN) factors in the axial and lateral directions, respectively. The weight function $w^{(i_s j_s)}$ is defined in such a way so that the RF windows of increasing distance from the interrogated window are least "emphasized". However, there is no constraint incorporated for the lesion edge preservation in the cost function (Eq. (8)). Thus, instead of a sharp change in the strain profile, a slowly decaying nature of the estimated strain is seen at the lesion edge regions.

2.2. Lesion edge preserved direct average strain estimation (LEP-DASE)

In detecting an edge along a line of intensity pixels, we may face two types of pixels: the noise pixel and the edge pixel (Fig. 1). A noise pixel is one which has much higher or lower intensity than the adjacent pixels having similar intensities. The edge pixel is one which is either on an inclining slope or on a declining. From these topology, we can define the following necessary parameters [14]:

$$D_x = \begin{cases} |I_E - I_W| - \delta; & \text{if} \quad |I_E - I_W| > \delta \\ 0; & \text{otherwise,} \end{cases} \tag{10}$$

$$A_X = \frac{1}{2}(I_E + I_W), \tag{11}$$

$$I'_{S,x} = \begin{cases} I_S - \frac{1}{2}D_X; & \text{if} \quad I_S > A_X \\ I_S + \frac{1}{2}D_X; & \text{if} \quad I_S \leqslant A_X, \end{cases} \tag{12}$$

$$P_X = I'_{S,x} - A_X, \tag{13}$$

where I_E and I_W represent the image intensity values at the east and west neighboring pixels, A_X represents the average of the neighbor-

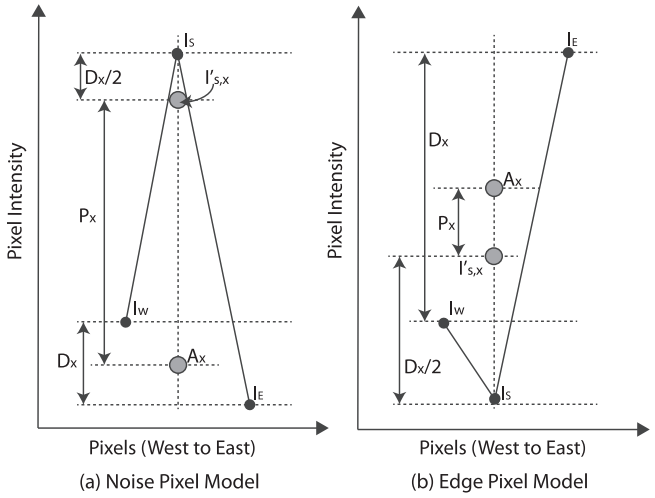

Fig. 1. Representation of (a) a typical noise pixel and (b) a typical edge pixel.

ing pixels in the x-direction (East–West), $I'_{S,x}$ is an intermediate intensity value of the interrogated pixel, and P_X is the difference between $I'_{S,x}$ and A_X. We define an auxiliary parameter $\delta \in [0, \sigma]$ to prevent small noise regions to be identified as edges, where σ is the standard deviation of the image noise. In the proposed method, median absolute deviation (MAD) is used for automatic computation of δ [5]. From Fig. 1, we see that P_X is greater than D_X for the noise-like pixel, and P_X is less than D_X for the edge-like pixel. For the y-direction (North-South), similar parameters $D_Y, A_Y, I'_{S,y}$, and P_Y can be estimated. These estimated parameters can be used for the edge detection in a whole intensity image.

As shown in Fig. 2, in the proposed method, we modify the edge detection scheme [14] originally designed for a whole intensity image. In Fig. 2a, we show a portion from the FEM simulation phantom (marked by a rectangular box "T" in Fig. 3b) having two different stiffness. The NCC peaks for the interrogated (i_s, j_s) and neighborhood tissue points for different stretching factor α are shown in Fig. 2b. It is expected that the window NCC peaks of different tissue points having similar stiffness will be maximized at the same stretching factor. Therefore, to check for the tissue points with identical stiffness to that of the interrogated tissue point, we need to find the reference stretching factor α_r at which the interrogated window NCC peak becomes maximum with respect to the stretching factor α and it can be estimated as

$$\alpha_r = \arg\max_{\alpha} \{\rho_{\alpha}^{(i_s, j_s)}\}. \tag{14}$$

Now, $M_{\alpha_r}(i_r, j_r)$ plane for $i_s - L_a \leqslant i_r \leqslant i_s + L_a$ and $j_s - L_l \leqslant j_r \leqslant j_s + L_l$ is considered as the reference image, and assumed equivalent to an intensity image for edge detection. A mesh plot showing the reference plane $M_{\alpha_r}(i_r, j_r)$ is depicted in Fig. 2(c). The region-of-interest (ROI) $(i_s - L_a \leqslant i_r \leqslant i_s + L_a$ and $j_s - L_l \leqslant j_r \leqslant j_s + L_l)$ that includes the interrogated and neighborhood tissue points consists of two homogeneous areas of highly different stiffness. Therefore, the compression factor in the post-compression signal windows inside this ROI will be much less in the stiffer area than the softer one. Note that the interrogated tissue point is on the border of the less stiff area (see Fig. 2a). In this case, since the NCC function between the interrogated pre-and post-compression signal windows will be maximum for the stretching factor α_r (Eq. (14)), the neighborhood NCC functions estimated from the corresponding pre-and post-compression windowed signals in the less stiff area of the ROI are also expected to be close to the maximum for the same stretching factor α_r due to their stiffness similarity to the interrogated one. However, using the same stretching factor α_r for the post-compression windowed signals in the stiffer area of the ROI will result in much lower NCC peaks as depicted in Fig. 2c. An informative NCC peak plane (i.e., the reference plane $M_{\alpha_r}(i_r, j_r)$) can, therefore, be formed as shown in Fig. 2c that has a very sharp edge at the interface of two dissimilar stiffness areas, where the edge detection scheme can be applied. Also note that instead of detecting edge in the entire $M_{\alpha_r}(i_r, j_r)$ plane, only the interrogated pixel (i.e., the NCC peak) is tested whether it is on an edge or not. The idea behind the edge detection on M_{α_r} is that if the interrogated pixel is on a lesion edge, P_X would be less than D_X and/or P_Y would be less than D_Y in $x-$ and $y-$ directions, respectively. Note that we calculate σ for the whole M_{α_r} plane.

Now the exponential weight defined in Eq. (9) needs to be modified to preserve the edge. The spreading of the exponential weight is to be controlled so that it does not include the smaller NCC values and thus, avoid interference of NCC values of different stiffer region into the cost function (Fig. 2c). However, from Eqs. (10)–(13), we can only know whether the interrogated NCC peak is on an edge or not, but we yet to know the orientation (i.e., East, West, North and South) of different stiffer region with respect to it. Let

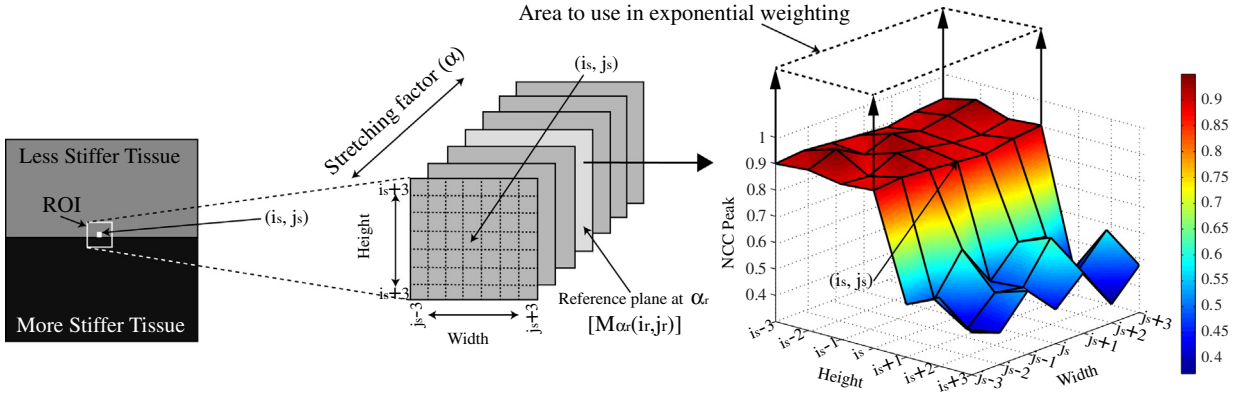

(a) A tissue scenario with two different stiffness creating an edge

(b) NCC peaks for different stretching factor, α

(c) Reference plane, M αr(ir,jr)

Fig. 2. Schematic and mesh diagrams illustrating the edge detection procedure, and tissue points selection for using in the exponential weighting. (a) A portion (as shown in Fig. 3b with dashed box "T") of the FEM simulation phantom with two different stiff areas creating an edge, (b) NCC peaks of the interrogated and neighborhood windows for different stretching factor, and (c) 2-D plot of the reference plane $M_{\alpha_r}(i_r, j_r)$.

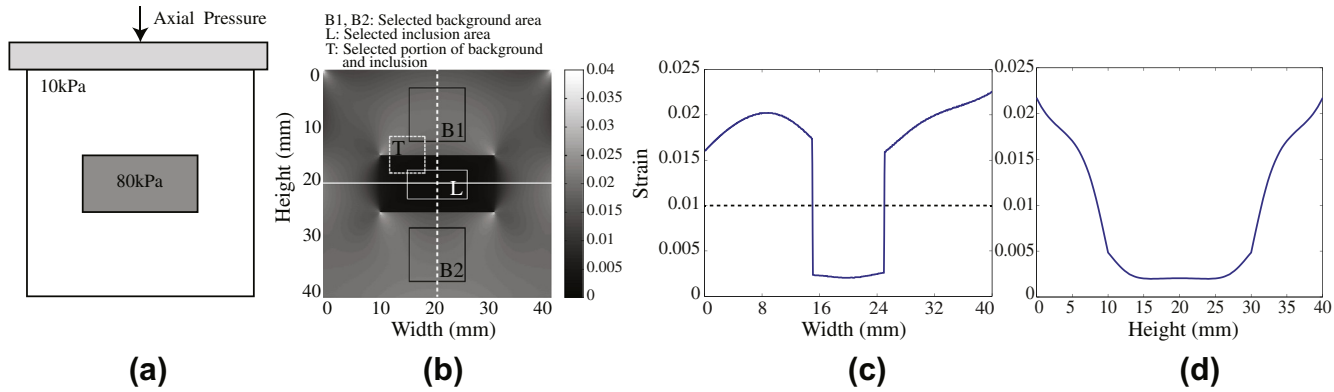

Fig. 3. FEM simulation phantom. (a) Stiff inclusions in a homogeneous background of 10 kPa, and (b) corresponding actual elastogram. (c) Strain profile of the vertical dashed line in (b), (d) strain profile of the horizontal solid line in (b).

the interrogated, East, West, North and South pixels are defined as $I=M_{\alpha_r}(i_s,j_s), E=M_{\alpha_r}(i_s,j_s+1), W=M_{\alpha_r}(i_s,j_s-1), N=M_{\alpha_r}(i_s-1,j_s)$ and $S=M_{\alpha_r}(i_s+1,j_s)$, respectively. Then, the modified ranges from East (R_E) to West (R_W) and North (R_N) to South (R_S) of the weight function defined in Eq. (9) can be chosen as

$$R_E=\begin{cases} j_s; & \text{if } |I-E|>|I-W| \\ j_s+L_l; & \text{otherwise,}\end{cases} \tag{15}$$

$$R_W=\begin{cases} j_s; & \text{if } |I-E|<|I-W| \\ j_s-L_l; & \text{otherwise,}\end{cases} \tag{16}$$

$$R_N=\begin{cases} i_s; & \text{if } |I-N|>|I-S| \\ i_s-L_a; & \text{otherwise,}\end{cases} \tag{17}$$

$$R_S=\begin{cases} i_s; & \text{if } |I-N|<|I-S| \\ i_s+L_a; & \text{otherwise.}\end{cases} \tag{18}$$

Now, by using these modified ranges for all the stretching factors, the modified cost function is defined for a particular strain point (i_s,j_s) on the strain map as

$$\tilde{J}_{\alpha}^{(i_s,j_s)}=\sum_{i_0=R_N}^{R_S}\sum_{j_0=R_W}^{R_E} w^{(i_s,j_s)}(i_0,j_0)M_{\alpha}(i_0,j_0). \tag{19}$$

Then, the desired value of α is calculated as

$$\alpha_o^{(i_s,j_s)}=\arg\max_{\alpha}\{\tilde{J}_{\alpha}^{(i_s,j_s)}\}. \tag{20}$$

And, finally, the effective average strain at (i_s,j_s) is estimated as

$$S_o(i_s,j_s)=1-\alpha_o^{(i_s,j_s)}. \tag{21}$$

3. Simulation and experimental results

We provide comparative results of our proposed method with the 2-D analytic minimization (AM2D) [21] and direct average strain estimation (DASE) [11] methods using the FEM phantom, experimental phantom (CIRS Inc., Norfolk, VA, USA) and the *in vivo* patient data. In addition to the evaluation by visual inspection, we compare the performances of different methods in terms of the SNRe [7], CNRe [24] and EMSE. The AM2D is a real-time elastography technique based on analytic minimization of a regularized cost function that incorporates similarity of RF data intensity and displacement continuity. The strain field is computed from the displacement field using Kalman filtering.

3.1. FEM simulation

A rectangular 40 mm × 40 mm FEM phantom was modeled using the analysis software ANSYS (ANSYS Inc., Canonsburg, PA, USA) and ultrasound simulation was performed over the model using Field II [12]. In this simulation, the total number of nodes was 54574. Due to using a 2-D model, it did not model out-of-plane motion. This phantom had a homogeneous background with stiffness of 10 kPa with a rectangular inclusion of dimension 10 mm × 20 mm (Fig. 3a). The stiffness of the inclusion was 80 kPa. The phantom was compressed from the top using a larger-width planar compressor. An ultrasonic transducer of *center frequency*, f_0 = 5 MHz and *band-width* = 50% was used to scan the phantom from the top. The total number of scan lines was 128.

For qualitative evaluation of the perceptual quality of the strain images generated by the AM2D, DASE and LEP-DASE methods, we present strain images of the FEM simulation phantom for three different applied strains (2%, 4% and 6%) in Fig. 4. For the DASE and LEP-DASE methods, we have used a data window (L_i) of 2.28 mm and an inter-window shift (L_v) of 0.28 mm. For all strains, all methods produce satisfactory strain images. However, strain images produced by the DASE and LEP-DASE methods are merely similar except the edge blurring performance. Due to no edge preserving constraint in the cost function-based average strain estimation of the DASE method, the inclusion edge is much blurred than that of the LEP-DASE method. This edge blurring effect can be well understood from the vertical 1-D strain profiles presented in Fig. 4j–l. The profiles are selected so that the variation of stiffness in the inclusion is included (dashed vertical line in Fig. 3b). In Fig. 4j–l, we see that the edges of the strain well produced by the DASE method are not enough steep compared to the actual ones resulting in a broadened transition width of the strain well due to blurring. On the other hand, we appropriately downsample the strain profile produced by the AM2D method to match the data length with that of the LEP-DASE and DASE methods. We can see from Fig. 4j–l that the strain profiles estimated by the proposed LEP-DASE method is more closer to the actual ones. For quantitative evaluation of the edge preserving performance, we calculate the EMSE between the actual and the estimated strain profiles, and also the inclusion width. The EMSE is calculated as

$$EMSE=\frac{1}{P}\sum_{p=0}^{P-1}[U(p)-V(p)]^2, \tag{22}$$

where U and V are the actual and estimated strain profiles of length P, respectively. On the other hand, the measured width of the inclusion at the width measuring line in Fig. 3c is 9.82 mm. We fit the width measuring line approximately at the mid-height of the strain

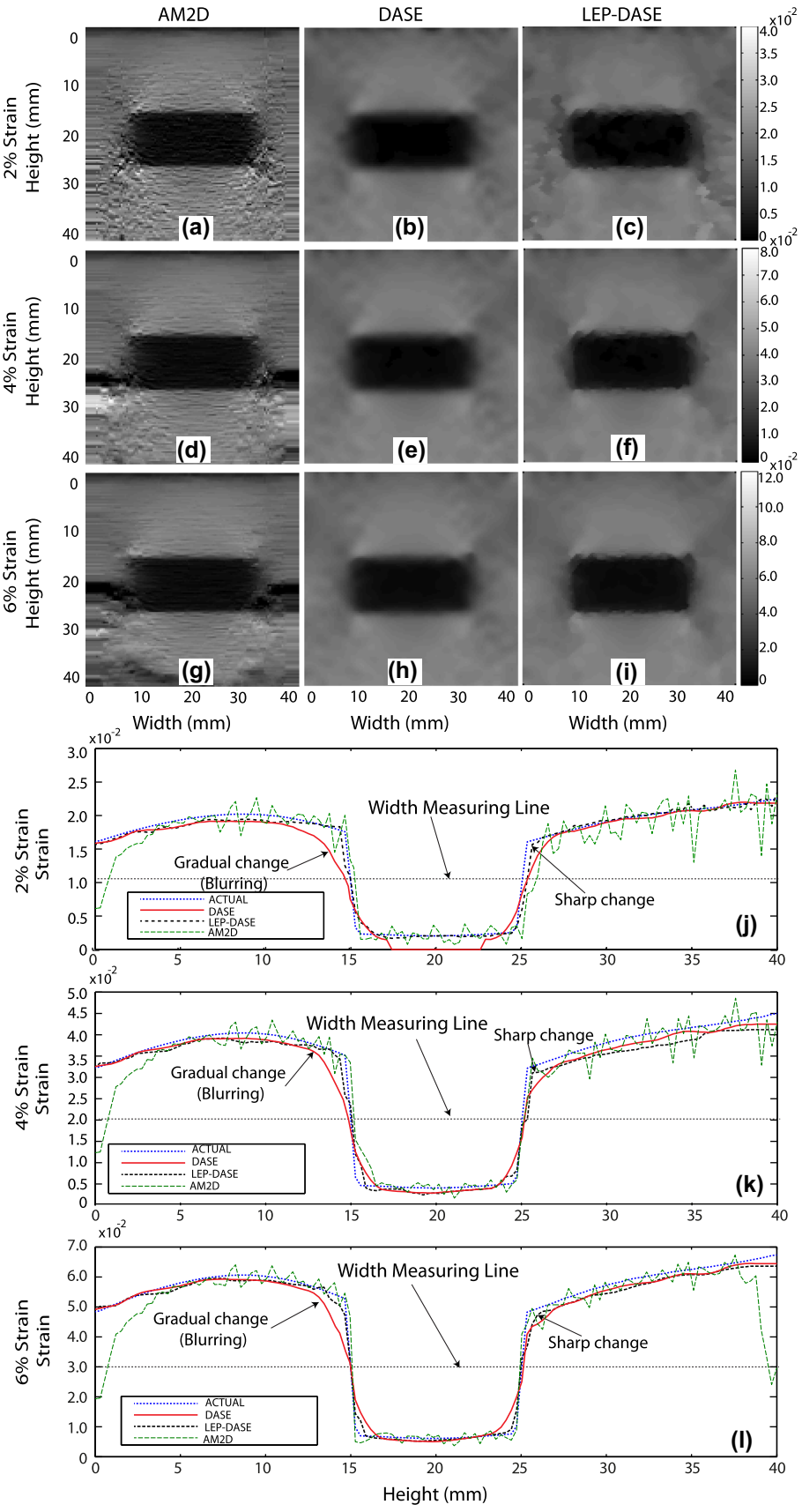

Fig. 4. Strain images of the FEM simulation phantom generated by different methods. Results (a, d, g) are produced by the AM2D, (b, e, h) are produced by the DASE ($L_a = 4$, $L_l = 4$, $\lambda_a = \lambda_l = 0.25$, $\nu = 0.5$), (c, f, i) are produced by the proposed LEP-DASE ($L_a = 4$, $L_l = 4$, $\lambda_a = \lambda_l = 0.25$, $\nu = 0.5$), and (j, k, l) represent the strain profiles of different methods at 2%, 4% and 6% applied strain, respectively.

Table 1
Estimated EMSE and inclusion widths for the stiffer inclusion at 2%, 4% and 6% applied strain. The actual inclusion width at the width measuring lines is 9.82 mm.

Methods	2% Strain		4% Strain		6% Strain	
	EMSE ($\times 10^{-5}$)	Width (mm)	EMSE ($\times 10^{-5}$)	Width (mm)	EMSE ($\times 10^{-5}$)	Width (mm)
AM2D	0.88	9.95	3.22	9.90	2.70	9.94
DASE	0.53	9.90	1.90	9.62	1.94	9.70
LEP-DASE	0.40	9.72	1.21	9.84	1.44	9.70

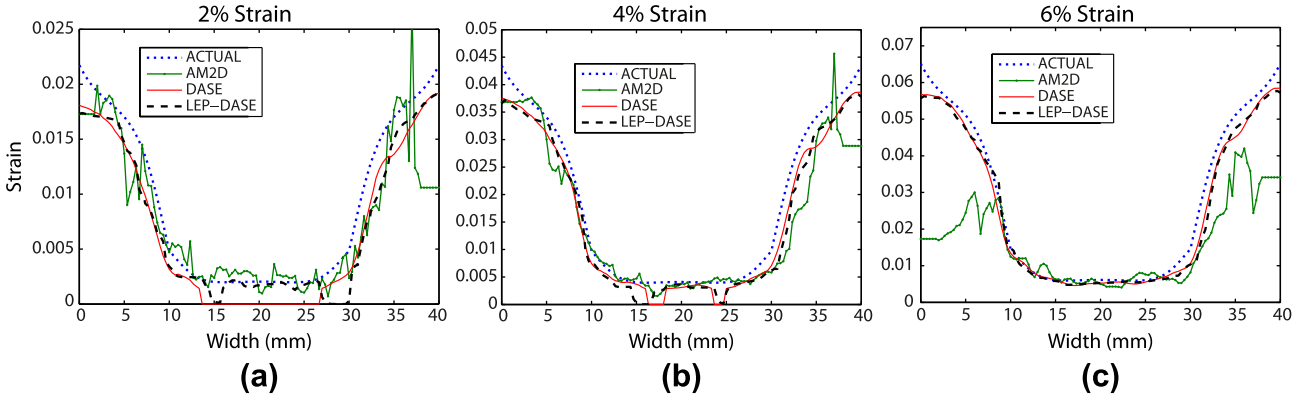

Fig. 5. Illustration of lateral strain profiles produced by the proposed, DASE and AM2D methods at (a) 2%, (b) 4%, and (c) 6% applied strain, respectively.

Table 2
SNRe and CNRe performance of different methods at 2%, 4% and 6% applied strain.

Methods	2% Strain		4% Strain		6% Strain	
	SNRe (dB)	CNRe (dB)	SNRe (dB)	CNRe (dB)	SNRe (dB)	CNRe (dB)
AM2D	19.73	19.86	22.92	23.74	24.53	25.30
DASE	26.28	28.20	26.71	27.61	27.07	28.90
LEP-DASE	26.00	27.46	26.38	27.01	26.84	28.61

well. The estimated values of EMSE and inclusion widths by different methods are shown in Table 1. Note that the presented EMSE values for all methods denote the minimum value obtained from the properly aligned actual and estimated strain profiles. It is evident that the estimated EMSE is the least for the proposed LEP-DASE method for all the three applied strain values. The EMSE performance of the AM2D method is the worst for all the cases. However, the estimated inclusion widths are fairly accurate for all the three methods.

We also show the horizontal 1-D strain profiles for the FEM simulation phantom at three different applied strains in Fig. 5. These profiles are selected in a way that the variation of stiffness in the inclusion is included (solid horizontal line in Fig. 3b). From Fig. 3d, it can be seen that the actual strain profile does not show sharp edges at the two sides of the inclusion. The estimated strain profiles in Fig. 5 by the DASE and LEP-DASE methods for 2%, 4%, and 6% applied strain satisfactorily follow the actual strain profile. But the strain profiles produced by the AM2D method at 2% and 4% applied strain have noticeable variations though following the actual trend while at 6% strain, it is significantly distorted (see Fig. 5a–c).

From Fig. 4, it may appear that the proposed LEP-DASE method preserves the inclusion edge at the cost of smoothing performance. Therefore, for quantitative performance evaluation of the proposed and other two methods, two numerical performance metrics (i.e., SNRe and CNRe) are calculated at different applied strain (e.g., 2%, 4% and 6%) for the FEM simulation phantom. The performance metric SNRe [7] is defined as

$$SNRe = \frac{\mu_s}{\sigma_s} \tag{23}$$

where, μ_s and σ_s denote the statistical mean and standard deviation of the strain computed in a homogeneous area, respectively. Similarly, the performance metric CNRe [24] is defined as

$$CNRe = \frac{2(\mu_l - \mu_b)^2}{\sigma_l^2 + \sigma_b^2} \tag{24}$$

where μ is the mean strain and σ is the standard deviation of the strain in a homogeneous area. The sub-subscript l and b refer to the inclusion and background, respectively. For estimating the SNRe and CNRe of the FEM simulation, the selected homogeneous background regions, B1 and B2, and the homogeneous inclusion area, L are shown in Fig. 3b with rectangular boxes. The calculated SNRe and CNRe values are presented in Table 2. From this Table, we can see that the SNRe and CNRe values of the strain images produced by the LEP-DASE method is pretty close to those of the DASE method although the SNRe and CNRe performance of the DASE method is the best among other methods. Nevertheless, the visual quality of the strain images by the LEP-DASE method appears to be better because of its lesion edge preserving performance (see Figs. 4, 6 and 7). The AM2D method shows the worst performance among the techniques compared with.

3.2. Experimental phantom results

We have used a tissue-mimicking (TM) experimental phantom of dimension 40 mm × 40 mm (CIRS Inc., Norfolk, VA, USA) to evaluate the performances of the proposed and other two techniques in this paper. The phantom has a homogeneous background of stiffness 33 kPa with an inclusion of stiffness 56 kPa inside. It was axi-

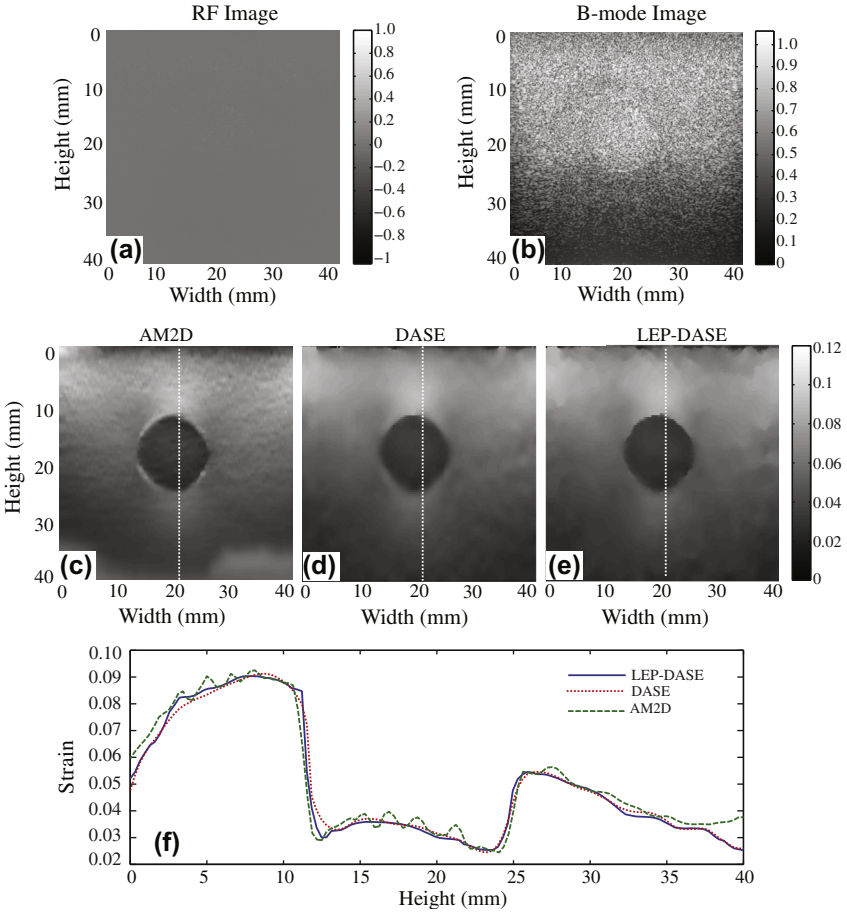

Fig. 6. Illustration of the B-mode and strain images of the experimental phantom generated by different methods at 6% applied strain: (a) RF image (Time-Gain-Compensation (TGC) is not used), (b) B-mode (TGC is not used), (c) AM2D, (d) DASE ($L_a = 4$, $L_l = 4$, $\lambda_a = \lambda_l = 0.25$, $v = 0.2$), (e) proposed LEP-DASE ($L_a = 4$, $L_l = 4$, $\lambda_a = \lambda_l = 0.25$, $v = 0.2$). (f) The strain profiles of different methods (white-dashed lines in (c–e)).

ally compressed 0.2 in. using a linear compressor which resulted in an average strain of 6%. An Antares Siemens system (Issaquah, WA, USA) with a 7.27 MHz linear array transducer was used to collect RF data at a sampling rate of 40 MHz.

We show the RF, B-mode, and strain images of the experimental phantom generated by the AM2D, DASE and LEP-DASE methods in Fig. 6. From this figure, we see that the strain images produced by the DASE and LEP-DASE methods are smoother than that of the AM2D method. However, the inclusion edge is seen blurred for the DASE method (Fig. 6d). But in Fig. 6e, we see that the inclusion edge is well preserved by the LEP-DASE method. We also show the strain profiles for the white-dashed lines in Fig. 6c–e in Fig. 6f. We appropriately downsample the strain profile produced by the AM2D method to match the data length with that of the LEP-DASE and DASE methods. From these strain profile plots, we see that the lesion edge is steeper for the LEP-DASE method than that of the DASE method while the profile produced by the AM2D method is not as smooth as those of the LEP-DASE and DASE methods.

Note that the lower 'semi-circle' of the inclusion in Fig. 6c–e is slightly more blurred than the upper one. This may be due to the fact that it resides in an area where the RF signal strength is significantly low due to depth and frequency dependent attenuation (see Fig. 6a and b plotted without any time-gain-compensation (TGC) of the RF data). The effect of interaction of the inclusion with the neighborhood due to axial compression might also be a cause of the little more blurring effect in that area. The second-half of the strain profiles shown in Fig. 6f also demonstrate this effect.

3.3. Comparison Using in vivo breast data

We have chosen three sets of *in vivo* breast data from an existing database of 194 cases (age: 14–63 years). These data were acquired by using a SonixTOUCH Research (Ultrasonix Medical Corporation, Richmond, BC, Canada) scanner integrated with a L14-5/38 probe operating at 10 MHz (nominal) at Bangladesh University of Engineering and Technology (BUET) Medical Center, Dhaka, Bangladesh. An institutional review board (IRB) approved the study. In addition, prior consent was taken from every patient for further use of these data in research. Note that data were acquired with free-hand compression of the ultrasound probe. Two of them represent benign breast tumors (Fibroadenoma) and the other one represents a malignant case. The B-mode images of patient-I (Age: 38/Tumor type: Fibroadenoma), patient-II (Age: 15/Tumor type: Fibroadenoma) and patient-III (Age: 25/Tumor type: Adenocarcinoma) are shown in Fig. 7a, e, and i, respectively.

We observe from Fig. 7 that the AM2D method smooths the lesions to such a degree for patient-I and II (Fig. 7b, and f) that the stiffness variation inside the lesions is totally lost. In case of patient-III, this method cannot perfectly extract the lesion from the background. In addition, because of the absence of any edge preserving constraint in the algorithm, the AM2D method smooths the lesion edges as well, which is clearly depicted in Fig. 7b. The DASE method though shows promise to be a better smoother, for the similar reason as stated above, it also smooths the lesion edges (Fig. 7c, g, and k). On the other hand, the proposed LEP-DASE meth-

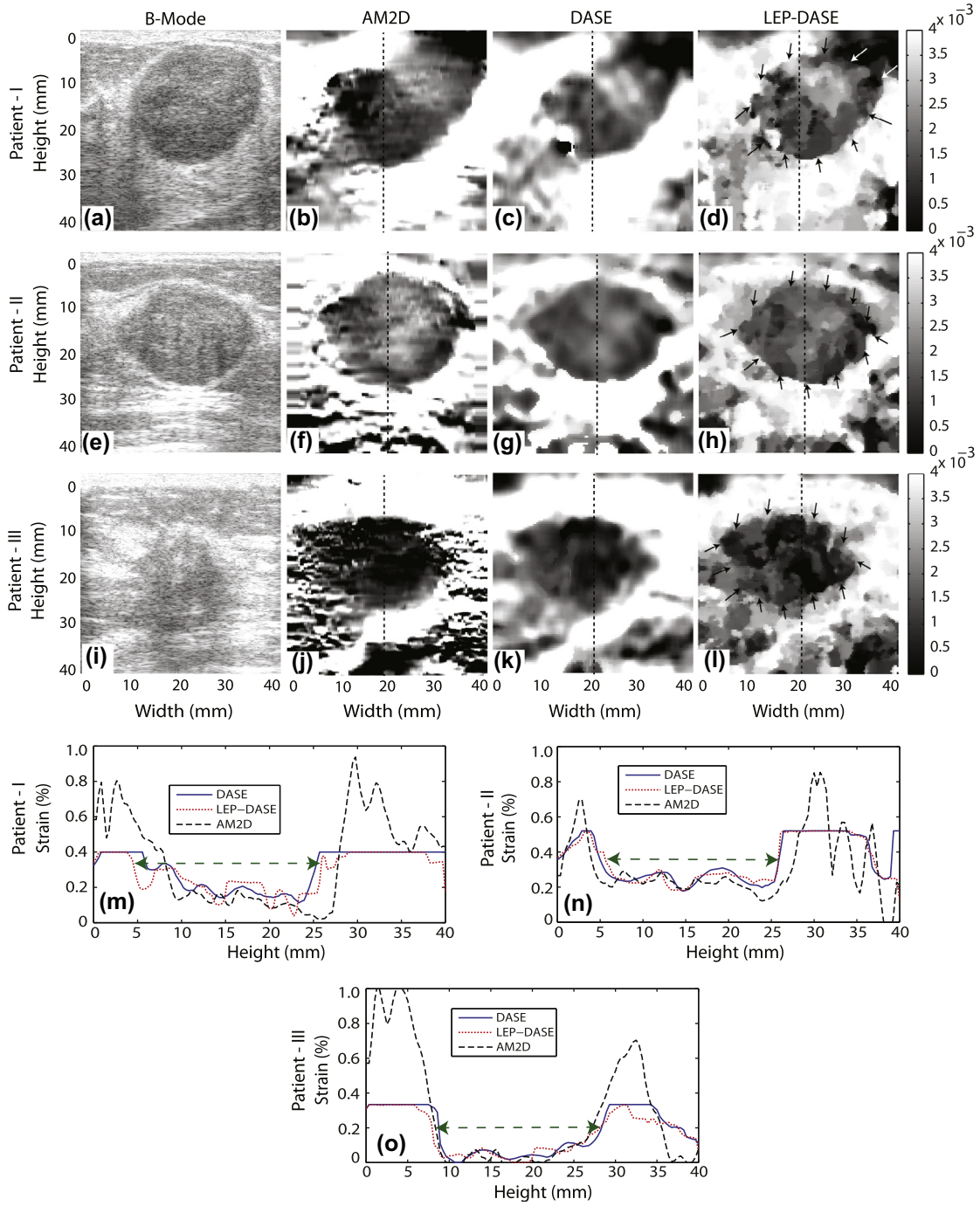

Fig. 7. B-mode images (a, e and i), and strain images of the *in vivo* breast data generated by different methods. Result (b, f and j) are produced by the AM2D, (c, g and k) are produced by the DASE ($L_a = 4$, $L_l = 4$, $\lambda_a = \lambda_l = 0.25$, $\nu = 0.5$), (d, h and l) are produced by the proposed LEP-DASE ($L_a = 4$, $L_l = 4$, $\lambda_a = \lambda_l = 0.25$, $\nu = 0.5$), and (m, n and o) represent the strain profiles of different methods (black-dashed lines in b–d, f–h and j–l for patient-I, II and III, respectively).

od smooths the strain images with the lesion edges preserved. In Fig. 7d, h, and l, we have traced the lesion edges with small arrows around them. As can be seen, the edges are much sharper and the smoothing of the stiffness variation inside the lesions is significantly less prominent than that of the original DASE method.

For better understanding of the lesion edge preservation scenario, we plot the 1-D strain profiles for patient-I, II and III in Fig. 7m–o, respectively. For each case, we see that the proposed LEP-DASE method produces a steeper edge on both sides of the lesions so that the lesion widths are clearly visible (indicated by arrows in Fig. 7m–o). Whereas the DASE method smooths the edge and the lesion width cannot be comfortably detected. On the other hand, the strain profiles produced by the AM2D method reveal that the strain well is not well-defined for the patient-I and II (Fig. 7m and n), and is satisfactory for detecting edges for the patient-III (Fig. 7o). We can also observe from the strain profiles produced by the proposed LEP-DASE method for the patient-I and II (Fibroadenoma) that the estimated strain inside the lesions is about 0.2% on average. Whereas for the patient-III (Adenocarcinoma), the estimated strain by the proposed LEP-DASE method inside the lesion

is almost close to zero. Thus, the typical assumption that malignant lesions are stiffer than benign ones hold true in this case.

3.4. Evaluating performance in terms of computation time

The computation time (CPU: Core i5, 2.3 GHz, RAM: 2 GB, software: MATLAB, The MathWorks, Natick, MA, USA) of our implementation of the AM2D, DASE, and LEP-DASE methods for generating the strain images (*in vivo* breast experiment: patient-I) was measured to be 0.35, 79.36, and 94.60 s, respectively. The results show that the AM2D method is very fast compared to others. However, the AM2D method uses mex files but the others do not. By using mex files, the computational time of the DASE and proposed method can also be reduced.

4. Discussion

The performance of the proposed LEP-DASE method has been demonstrated both quantitatively and qualitatively in the results section. The distinct feature of the proposed LEP-DASE method that differentiate it from the other strain continuity ensuring methods, such as [10,11,21] is the detection of inclusion/lesion edges prior to strain estimation and the formulation of the cost function accordingly in a way that the inclusion/lesion edges are well preserved while ensuring strain continuity among the neighborhood tissues. The perceptual quality of the strain image obtained by the proposed LEP-DASE method, in particular for the *in vivo* patient data, has improved significantly in the lesion area due to the reduction of the blurring effect. However, the computational complexity of the LEP-DASE method is slightly higher than that of the DASE due to incorporation of the edge detection algorithm, as it requires some extra processing for each interrogated signal windows. Unlike the DASE and LEP-DASE methods, the AM2D is a real-time elastography method due to its high computational efficiency.

To compensate for the lateral shift of the RF data without using a 2-D search region, the Poisson's ratio, v has been used in Eq. (4) to save some extra computation [10]. It has been varied from 0 to 1 at an interval of 0.25 in order to choose an appropriate value and the optimum image quality for all the strain images shown has been observed for $v = 0.5$. This value agrees with that reported in [6]. In addition, it is assumed that $p(\alpha t) \cong p(t)$ while similarity between $r_1^{(i_s j_s)}$ and $r_\alpha^{(i_s j_s)}$ is computed in Eq. (6). However, this assumption is reasonably accurate at low strain [2,3]. Further study on the estimation of PSF ($p(t)$) is necessary to compensate for this effect.

As the ultrasound RF signal gets attenuated while propagating along depth, the signal-to-noise ratio decreases. However, this attenuation effect is less observed in the correlation-based techniques (i.e., DASE and proposed LEP-DASE) as these methods seek for the RF waveform similarity between the the pre- and post-compression signal windows. On the contrary, as the AM2D method is based on pixel intensity similarity between the pre-and post-compression signals, it is highly sensitive to ultrasound attenuation effect. Moreover, the algorithm has been observed to be highly sensitive to setting of the several other parameters.

The proposed LEP-DASE method enhances the ultrasonic average strain imaging performance particularly by delineating the lesion edge more clearly as compared to other contemporary techniques. The lesion edge preserved strain imaging might be clinically significant for classifying tumors based on their shape and area ratio (elastographic to B-mode) and also for determining the spatial extent of tumors.

5. Conclusions

In this paper, we have presented a lesion edge preserving direct average strain estimation method for high quality quasi-static elasticity imaging. To prevent blurring of the lesion edge while ensuring strain continuity, an intelligent edge preservation criterion is incorporated in the exponential weighting process of the strain determining cost function. It has been shown by the simulation, experimental and *in vivo* patient results that the proposed method is more accurate and robust in edge preservation than the other recently reported strain estimation methods that have been designed to ensure strain continuity.

Acknowledgements

This work has been supported by HEQEP UGC (CP#96/BUET/Win-2/ST (EEE)/2010), Bangladesh, and in part by National Research Foundation of Korea (NRF) grant funded by the Korea government (No: 2009-0078310).

References

[1] S.K. Alam, Novel spline-based approach for robust strain estimation in elastography, Ultrason. Imag. 322 (2010) 91–102.
[2] S.K. Alam, F.L. Lizzi, T. Varghese, E.J. Feleppa, S. Ramachandran, Adaptive spectral strain estimators for elastography, Ultrason. Imag. 263 (2004) 131–149.
[3] S.K. Alam, J. Ophir, E.E. Konofagou, An adaptive strain estimator for elastography, IEEE Trans. Ultrason. Ferroelect. Freq. Contr. 452 (1998) 461–472.
[4] M. Bilgen, M.F. Insana, Deformation models and correlation analysis in elastography, J. Acoust. Soc. Am. 995 (1996) 3212–3224.
[5] M.J. Black, G. Sapiro, D. Marimont, D. Heeger, Robust anisotropic diffusion, IEEE Trans. Image Process. 7 (1998) 421–432.
[6] E. Brusseau, C. Perrey, P. Delachartre, M. Vogt, D. Vray, H. Ermert, Axial starin imaging using local estimation of the scaling factor from RF ultrasound signals, Ultrason. Imag. 22 (2000) 95–107.
[7] E.I. Céspedes, J. Ophir, Reduction of image noise in elastography, Ultrason. Imag. (1993) 152.
[8] E.I. Céspedes, J. Ophir, H. Ponnekanti, N. Maklad, Elastography: elasticity imaging using ultrasound with application to muscle and breast in vivo, Ultrason. Imag. 152 (1993) 73–88.
[9] B.S. Garra, E.I. Céspedes, J. Ophir, S.R. Spratt, R.A. Zuurbier, C.M. Magnant, M.F. Pennanen, Elastography of breast lesions: initial clinical results, Radiology 202 (1997) 79–86.
[10] M.K. Hasan, E.M.A. Anas, S.K. Alam, S.Y. Lee, Direct mean strain estimation for elastography using nearest-neighbor weighted least-squares approach in the frequency domain, Ultrason. Med. Biol. 38 (2012) 1759–1777.
[11] M.A. Hussain, E.M.A. Anas, S.K. Alam, S.Y. Lee, M.K. Hasan, Direct and gradient-based average strain estimation by using weighted nearest neighbor cross-correlation peaks, IEEE Trans. Ultrason. Ferroelect. Freq. Contr. 598 (2012) 1713–1728.
[12] J.A. Jensen, Field: a program for simulating ultrasound systems, in: 10th Nordicbaltic Conf. on Biomed. Imag. 4, 1996, 351–353.
[13] F. Kallel, J. Ophir, A least-squares strain estimator for elastography, Ultrason. Imag. 193 (1997) 195–208.
[14] E. Michel-González, M.H. Cho, S.Y. Lee, Geometric nonlinear diffusion filter and its application to X-ray imaging, BioMed. Eng. OnLine 10 (2011).
[15] J. Ophir, S.K. Alam, B.S. Garra, F. Kallel, E.E. Konofagou, T. Krouskop, C.R.B. Merritt, R. Righetti, R. Souchon, S. Srinivasan, T. Varghese, Elastography: imaging the elastic properties of soft tissues with ultrasound, J. Med. Ultrasound 29 (2002) 155–171.
[16] J. Ophir, S.K. Alam, B.S. Garra, F. Kallel, E.E. Konofagou, T. Krouskop, T. Varghese, Elastography: ultrasonic estimation and imaging of the elastic properties of tissues, J. Eng. Med. 2133 (1999) 203–233.
[17] J. Ophir, E.I. Céspedes, B.S. Garra, H. Ponnekanti, Y. Huanga, N. Maklad, Elastography: ultrasonic imaging of tissue strain and elastic modulus in vivo, Eur. J. Ultrasound 31 (1996) 49–70.
[18] J. Ophir, E.I. Céspedes, H. Ponnekanti, Y. Yazdi, X. Li, Elastography: a quantitative method for imaging the elasticity of biological tissue, Ultrason. Imag. 13 (1991) 111–134.
[19] B. Pan, K. Qian, H. Xie, A. Asundi, Two-dimensional digital image correlation for in-plane displacement and strain measurement: a review, Meas. Sci. Technol. 20 (2009) 062001.
[20] C. Pellot-Baraka, F. Frouin, M.F. Insana, A. Herment, Ultrasound elastography based on multiscale estimations of regularized displacement fields, IEEE Trans. Med. Imag. 232 (2004) 153–163.
[21] H. Rivaz, E.M. Boctor, M.A. Choti, G.D. Hager, Real-time regularized ultrasound elastography, IEEE Trans. Med. Imag. 304 (2011) 928–945.

[22] H. Rivaz, E.M. Boctor, P. Foroughi, R. Zellars, G. Fichtinger, G.D. Hager, Ultrasound elastography: a dynamic programming approach, IEEE Trans. Med. Imag. 2710 (2008) 1373–1377.
[23] T. Varghese, E.E. Konofagou, J. Ophir, S.K. Alam, M. Bilgen, Direct strain estimation in elastography using spectral cross-correlation, Ultrasound Med. Biol. 269 (2000) 1525–1537.
[24] T. Varghese, J. Ophir, An analysis of elastographic contrast-to-noise ratio performance, Ultrasound Med. Biol. 246 (1998) 915–924.
[25] R. Zahiri-Azar, S.E. Salcudean, Motion estimation in ultrasound images using time domain cross correlation with prior estimates, IEEE Trans. Biomed. Eng. 5310 (2006) 1990–2000.